Mobility of twinning dislocations in copper up to supersonic speeds

Ta Duong[1*], Rémi Dingreville[2], Michael J. Demkowicz[1]
[1]Department of Materials Science and Engineering, Texas A&M University, College Station, TX, 77843
[2] Center for Integrated Nanotechnologies, Sandia National Laboratories, Albuquerque, NM 87123

*Corresponding author: ddinhta@tamu.edu

Abstract:
Understanding the mobility of twining dislocation is important for multiscale modelling of crystal plasticity, especially at high strain rates, where such dislocations may reach transonic or supersonic speeds. We used molecular dynamics simulations to investigate the relationship between dislocation velocity and the applied resolved shear stress of an edge twinning dislocation in copper up to supersonic speeds. The twinning-dislocation mobility relation is composed of two branches separated by a band of forbidden velocities. The lower velocity branch is limited by the first transverse sound speed ~2000 m/s while the upper branch stretches from ~3500 m/s in the transonic regime to supersonic velocities. Twinning dislocations cannot undergo uniform steady-state motion at velocities within the forbidden band. Our simulation results also reveal that edge twinning-dislocation motion in copper is kink-mediated. We discuss the implications of our findings for the motion of twins, twinning dislocations, and twinning-dislocation kinks in copper.

1. Introduction

Several studies suggested that twins in crystalline solids may move at velocities comparable to the speeds of sound. In high strain rate loading of an aluminum alloy (Al-4.8 wt% Mg), Gray estimated that twins move at ~3000 m/s, which is close to the lower transverse sound speed in Al (3160 m/s) [1]. Similarly, Faran and Shilo investigated twin growth driven by electric fields in barium titanate ($BaTiO_3$) [2] and reported a twin velocity of ~5200 m/s, or 1.16 times the transverse sound speed. Since deformation twinning usually proceeds through the propagation of twinning dislocations (TDs) on coherent twin boundaries [3], the foregoing studies imply that TDs may also move at sonic speeds or above.

The relationship between dislocation glide velocity v and the applied resolved shear stress τ in the Burgers vector direction is known as the mobility relation [4]. For $v < \sim 10^2$ m/s, dislocation mobility may be investigated by the etch pit method of Johnston and Gilman [5]. It has been applied to pure copper (Cu) [6-9] and to Cu alloys [10, 11]. However, higher dislocation speeds remain difficult to probe experimentally. The highest velocity observed by the etch pit method is half the lower transverse sound speed in lithium fluoride (LiF) [12]. Nosenko *et al.* performed optical observations of supersonic dislocations in an ordered suspension of charged dust particles [13], which was considered as a surrogate for a crystalline solid. Recent developments in x-ray radiography have led to reports that partial dislocations in diamond reach speeds in excess of 18 km/s [14]. However, these experiments are not yet able to determine the full mobility relation for individual dislocations.

In the absence of experiments, numerical simulations such as molecular dynamics (MD) and dislocation dynamics (DD) have been used to investigate dislocation mobility and its effect on

crystal plasticity. While numerous MD studies have been dedicated to sonic, transonic, and supersonic dislocations in single crystals [15-22] with maximum velocities near and above 3000m/s, the motion of TDs at such velocities has received comparatively little attention. Daphalapurkar *et al.* [23] investigated TD motion in Ni and found that it shares features in common with the mobility of dislocations in single crystal Ni [15]. However, they observed that, unlike dislocations in single crystals, TDs may move at supersonic speeds, *i.e.*, faster than the longitudinal sound speed. Nevertheless, Daphalapurkar *et al.* did not obtain the full mobility relation for TDs. Wei and Peng [24] studied the stress-velocity relationship of TDs in Cu and observed two limiting speeds in the transonic and supersonic regimes. However, due to the short time of their simulations (<100 ps), they did not obtain the full mobility relation, either. Other research groups modeled the glide of multiple TDs [25, 26] with a view to understanding the motion of incoherent twin boundaries, rather than individual TDs. Obtaining the twin mobility relation and comparing it to that of dislocations in single crystals is one of the main goals of the present study.

DD studies have also been carried out to investigate the interaction of dislocations traveling at transonic and supersonic velocities [27-29], with a focus on understanding how dislocation mobility changes the deformation response of a representative volume element. For instance, Cho and coworkers [30] showed that dislocation mobility laws that distinguish two velocity regimes play an important role in the evolution of a dislocation network in Al. Similarly, Gurrutxaga-Lerma [31] showed the influence that different inertial dislocation mobility laws have on the velocity of dislocations in Al crystals and their associated effects on plastic relaxation. Cui and coworkers [29] used DD simulations to study stress interactions between subsonic and supersonic dislocations. However, a unique mapping between the response of a representative volume and the form of the mobility relation is not available, necessitating investigation of individual dislocation behavior. Conversely, improved understanding of the mobility of individual dislocations stands to advance predictive modeling of crystal plasticity at high strain rates.

The goal of the present study is to investigate the motion of sonic, transonic, and supersonic TDs with a view to improving understanding of twinning during high strain rate deformation. We choose Cu as a model material for the present work because a reliable embedded atom method (EAM) [32] potential is available for it and because the mobility of dislocations in face-centered cubic (FCC) Cu, as modeled using this potential, is well understood [33]. Indeed, it has already been established that the mobility relation of straight glide dislocations in Cu is composed of multiple ranges of stable uniform motion separated by bands of forbidden velocity [33]. Moreover, edge and screw dislocations have different mobility relations. These findings further motivate investigations of TD mobility, as TDs have different structure than glide dislocations in grain interiors. The TD in our study is a pure edge Shockley partial propagating on a Σ3 coherent twin boundary (CTB). Deformation twinning through TD propagation along Σ3 CTBs is common in Cu [34] and Cu-base alloys [35, 36]. Thus, our findings relate directly to high-speed twin propagation in these materials: if the density and velocities of TDs on a twin boundary are known, the velocity of the twin boundary may be calculated.

Section 2 describes the atomistic models of a pure edge TD and methods for simulating its glide at different velocities. In Section 3, we present the mobility relation of a TD. Homogeneous dislocation nucleation in the CTB is also discussed. Section 4 reports on kink-mediated TD motion, revealed by our MD simulations. Finally, Section 5 presents the relationship between kink, TD, and CTB motion, compares mobility relations of edge, screw, and twinning dislocations in Cu, and discusses prospects for experimental measurements on high-speed TDs. We summarize our main conclusions in Section 6.

2. Modeling methods

We used the Large-scale Atomic/Molecular Massively Parallel Simulator (LAMMPS) code [37] to perform our MD simulations of a twinning dislocation gliding along a coherent twin boundary in copper. Interatomic forces were represented with the EAM [38] potential by Mishin *et al.* [32]. This potential is well tested in prior dislocation mobility simulations [33, 39]. Visualizations were performed using OVITO [40]. We investigated the three models shown in Fig. 1: a perfect CTB, a straight TD, and a TD with a pre-existing kink. The models are provided as supplementary files with this publication. All models are relaxed to zero pressure at a temperature of 10 K. Analysis of local atomic structures is performed by common neighbor analysis (CNA) [41].

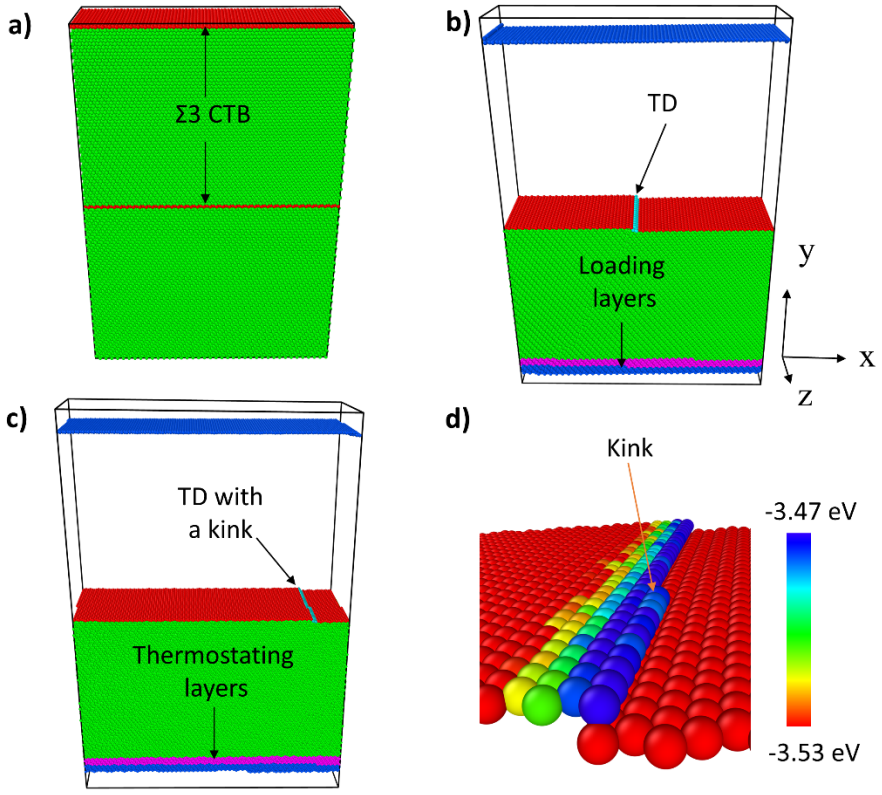

Figure 1: Models of a) perfect Σ3 CTBs, b) a straight edge TD, and c) an edge TD with a kink. Based on CNA, perfect FCC atoms are in green, CTB in red, TD in cyan. All FCC atoms in the upper grain in b) and c) are suppressed to show the CTB plane. d) Close-up view of a kink with atoms colored by their potential energy. The loading layers in blue and thermostatting layers in magenta imposed on the bottom surface are shown in b) and c), respectively. Loading and thermostatting layers are also imposed on the top surface, but, for clarity, they are not marked.

2.1. Coherent twin boundary

Figure 1.a) presents a perfect CTB consisting of two FCC Cu crystals joined along the (111) plane, whose normal direction is aligned with the y-axis of the simulation cell. The $[11\bar{2}]$ and $[1\bar{1}0]$ crystallographic directions within the CTB plane are parallel to the x- and z-axes, respectively. Periodic boundaries are applied in all three directions, so the model contains two parallel CTBs,

as shown in Fig. 1.a). The CTB energy, γ_{CTB}, is computed as the excess energy in the Gibbsian sense,

$$\gamma_{CTB} = \frac{PE - NE_{coh}}{2A} = 22.4 \text{ mJ/m}^2, \quad (1)$$

where A is the area of one CTB, PE is the total potential energy of the model, N is the number of atoms in the model, and $E_{coh} = -3.54$ eV is the cohesive energy per atom of a FCC Cu single crystal. The γ_{CTB} value we obtained is consistent with that measured in experiments (~20mJ/m^2) [42] and prior atomistic calculations (22.2 mJ/m^2) [43] using the same interatomic potential.

2.2. Straight twinning dislocation

Figure 1.b) shows a model of a straight edge TD on a CTB. To construct this model, we began with the perfect CTB in Fig. 1.a) and removed the periodic boundary along the y-axis. Consequently, the TD model terminates with free surfaces perpendicular to the y-axis. Boundary conditions remain periodic in the z- and x-directions. To introduce a TD, a net closure failure equal to that of a single edge Shockley partial dislocation must be created by removing $(11\bar{2})$ planes from the model.

To that effect, we reduced the length of the crystal above the CTB in the x-direction by removing four $(11\bar{2})$ atomic planes, *i.e.*, double the length of a Shockley partial Burgers vector ($2a/\sqrt{6}$, where a is the cubic lattice parameter). We also reduced the length of the crystal below the CTB plane along the x-direction by removing two $(11\bar{2})$ atomic planes, *i.e.*, one length of a Shockley partial Burgers vector ($a/\sqrt{6}$). The resulting net closure failure is that of one Shockley partial Burgers vector ($a/\sqrt{6}$). The reason why constructing a TD model requires removal of $(11\bar{2})$ planes from both the crystals above and below the CTB is explained in Appendix A. In short, a perfect stacking sequence below and above the CTB plane may only be recovered for certain combinations of $(11\bar{2})$ planes removed from the crystals above and below the CTB. This constraint arises from the nature of the $(11\bar{2})$ stacking sequence in FCC crystals.

After these operations, the crystal above the CTB plane is shorter than that below the CTB plane by one Shockley partial Burgers vector magnitude along the x-direction. However, merely reducing the length of the model in the x-direction results in incorrect stacking of $(11\bar{2})$ atomic planes under periodic boundary conditions. As explained in Appendix A, to recover the correct stacking, we must change the simulation cell from orthorhombic to triclinic by tilting the x-direction continuation vector in the y-direction by $a/\sqrt{3}$ (one atomic plane distance in the y-direction). This operation recovers the perfect FCC crystal structure in both the upper and lower parts of the model while forming a step at the CTB. A single terrace step is created on each free surface in the model, as well. We also adjust the model dimensions to relax the normal stress in the x-direction.

We used the Burgers circuit construction to verify the character of the TD. A closed circuit is drawn around the TD and compared with the corresponding circuit drawn in the perfect CTB model, following the FS/RH convention [4]. The closure failure in the CTB model is $\frac{a}{6}[11\bar{2}]$, confirming that the TD has the Burgers vector of a pure edge Shockley partial. We identified atoms in the TD core as those with potential energy greater than -3.53 eV which is just in excess of the cohesive energy of a bulk Cu atom. By this criterion, the TD core is four atom rows wide, as illustrated in Fig. 1.d). To compute the TD energy per unit length, δ_{TD}, we selected a layer of

atoms from the middle of the model that contains the entire CTB and TD, but no surface atoms. From the total potential energy PE and number of atoms N_{TD} of the layer, we compute

$$\delta_{TD} = \frac{PE - N_{TD}E_{coh} - \gamma_{CTB}A}{L} = 0.33\,\frac{eV}{\text{Å}}, \qquad (2)$$

where L is the TD length.

2.3. Twinning dislocation with a pre-existing kink

Finally, Fig. 1.c) shows a model of an edge TD with a kink on it. To construct this configuration, we began with the model of a straight edge TD shown in Fig. 1.b). We then tilted the z-axis continuation vector by $a/\sqrt{6}$ in the x-direction. Under periodic boundary conditions, this tilt changes the line direction of the TD by one atom row spacing: just enough to create one kink. The kink may be viewed as a point defect on the TD line. To compute its formation energy, ε_{kink}, we considered a layer containing the entire TD (including the kink) and CTB. Then,

$$\varepsilon_{kink} = PE - N_{kink}E_{coh} - \gamma_{CTB}A - \delta_{TD}L = 1.13\,\frac{eV}{kink}, \qquad (3)$$

where PE is the total potential energy of the layer and N_{kink} is the number of atoms in the layer.

As will be shown in section 3, glide of the TD causes the CTB to migrate. The models in Fig. 1 have dimensions ~ 26.3×25×8 nm^3. However, to maximize the distance that the CTB can move within a single simulation, we also constructed models with larger length along the y-direction: 113 nm (rather than 25 nm). The CTB in these models is constructed at an initial location close to the bottom surface (within 20 nm of the bottom surface) and allowed to approach the upper surface (within 20 nm of the top surface) in loading simulations.

2.4. Loading and velocity calculations

Simulations of dislocation motion were carried out within the microcanonical (NVE) ensemble at an initial temperature of 10 K. To force the TD to move, we sheared the model at a constant strain rate by imposing a constant velocity $v_{loading}$ in the x-direction on a pre-selected layer of atoms (a "loading layer") located on the top surface and an equal and opposite velocity -$v_{loading}$ on another layer of atoms located on the bottom surface, as illustrated in Fig. 1.b). Only the center of mass velocities of these loading layers were constrained, allowing the surfaces to remain flexible. Immediately adjacent to the loading layers, we defined thermostatting layers, illustrated in Fig. 1.c), whose temperature was kept fixed at 10 K by rescaling the velocity every 0.1 ps. These layers served as sinks for heat generated at the dislocation core by the dissipation of external plastic work done on the model. A detailed description of the implementation of loading and thermostatting layers is given in Ref. [33].

Given a fixed dislocation density, the average TD velocity may be computed using the Orowan relation [44]: $\bar{v}_{TD} = \frac{2L_x}{b} v_{loading}$, where L_x is the length of simulation cell in the x-direction and b is the magnitude of the Burgers vector. In our models, this relation predicts that the TD moves at an average speed ~180 times greater than $v_{loading}$. We determine the instantaneous velocity

v_{inst} of the TD as $v_{inst} \approx \frac{\Delta x}{\Delta t}$, where Δx is TD displacement during time interval Δt, with typical Δt = 2 ps. The displacement Δx is obtained by tracking the position of the TD as a function of time. TD position is the average of the positions of all atoms in the TD core, as identified by CNA [41]. The instantaneous shear stress σ_{xy} on a loading layer is the total force in x-direction acting on all atoms from the loading layer divided by the area (along the x-z plane) of the layer. This shear stress is equal to the resolved stress acting on the TD in our simulations.

To aid in the analysis of TD mobility, we used continuum anisotropic linear elasticity theory to compute different characteristic velocities of Cu, in the direction of TD motion, *i.e.*, $[11\bar{2}]$. These velocities include the Rayleigh wave speed (1975 m/s); the lower transverse sound speed (2012 m/s); the higher transverse sound speed (2650 m/s); and the longitudinal sound speed (5028 m/s). Methods for calculating these velocities are described in Refs. [33, 45, 46].

3. Twinning dislocation mobility relation

Similar to dislocations in single crystal FCC Cu [33], TDs exhibit three types of motion, depending on the predicted average velocity, $v_{predict}$: uniform steady-state motion, cyclic steady-state motion, and homogeneous nucleation. Uniform motion occurs whenever $v_{predict}$ lies below 1990m/s as well as in the range ~3500 m/s <$v_{predict}$< ~ 5600 m/s. Figure 2.a) shows velocity and shear stress as a function of time for uniform motion at $v_{predict}$= 1430 m/s. After a transient period of ~300 ps, the TD moves with instantaneous velocity that oscillates around a steady state value of 1428 ± 4 m/s, consistent with the predicted velocity. Shear stress also oscillates about a steady state value. Uniform motion at other values of $v_{predict}$ exhibit velocities and stresses qualitatively similar to those in Fig. 2.a).

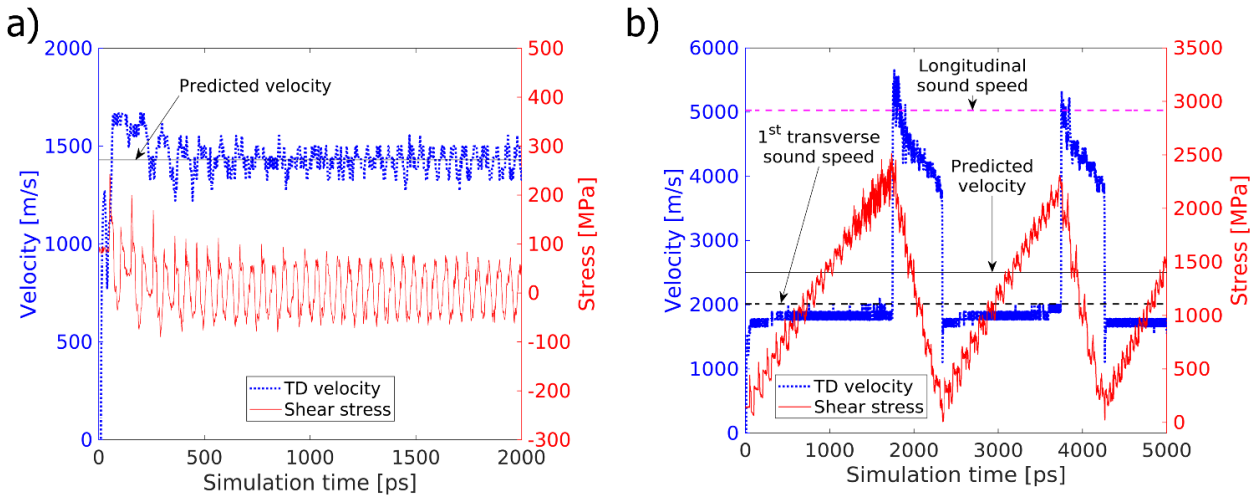

Figure 2: a) Uniform motion at $v_{predict}$=1430m/s. Here the TD velocity oscillates about the predicted velocity while the shear stress oscillates about 12MPa. b) Cyclic motion at $v_{predict}$=2503m/s. Here, the TD undergoes discrete jumps between low and high velocity branches. The shear stress increases while the dislocation is in the lower velocity branch and decreases while the dislocation is higher velocity branch. Both velocity and stress vary cyclically with the same approximate period.

Each time a TD traverses the length L_x of the simulation cell, the CTB moves by one interatomic plane spacing $a/\sqrt{3}$ in the positive y-direction. Thus, the CTB continually migrates in our simulations. For example, Fig. 3 shows snapshots of the CTB at $t = 0$ ns, $t = 3$ ns and $t = 6$ ns in a simulation with $v_{predict}$=1430 m/s. In this simulation, the CTB moves in the y-direction at an average speed of ~11 nm/ns.

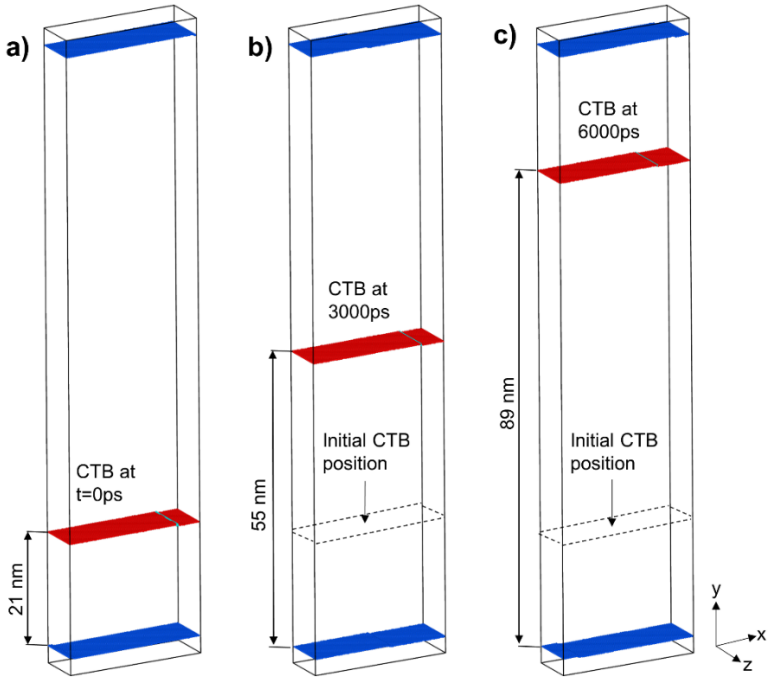

Figure 3: CTB migration in a simulation with the TD moving at predicted velocity =1430 m/s: a) $t = 0ns$ (initial position), b) $t = 3ns$, and c) $t = 6ns$.

Cyclic motion occurs whenever ~2000 m/s $< v_{predict} <$ ~3500 m/s. Figure 2.b) shows an illustrative example of TD velocity and shear stress variation as a function of time for $v_{predict}$=2503 m/s. At the beginning of the simulation, the TD accelerates rapidly and approaches asymptotically to ~2000 m/s. After ~1.8 ns, the dislocation jumps to supersonic speed, with v_{inst} ≈5600 m/s. Over the next ~2.2 ns, TD velocity gradually decreases to ~3500 m/s, whereupon it drops suddenly to just below ~2000 m/s. Thereafter, these velocity variations repeat cyclically. While the v_{inst} never equals $v_{predict}$, the average of v_{inst} over one cycle is 2499 ± 25 m/s, consistent with predicted velocity.

The resolved shear stress also undergoes cyclic variations, correlated with variations in TD velocity. While $v_{inst} < v_{predict}$, the rate of plastic strain accumulated due to dislocation motion is lower than the total externally imposed strain rate. Thus, the net elastic strain rate is positive and shear stress increases monotonically. Conversely, when $v_{inst} > v_{predict}$, the plastic strain rate is greater than the total strain rate. Consequently, the net elastic strain rate is negative and shear stress decreases monotonically. Cyclic motion has also been reported in simulations of dislocation mobility in Cu [33] and Ag [47].

Whenever $v_{predict}$ >5600 m/s, we observe homogeneous nucleation of dislocation loops along the CTB plane, as illustrated in Fig. 4. As these loops expand, they interact with their periodic images and coalesce into new TDs spanning the width of the model. These simulations involve multiple dislocations moving along the CTB at different velocities, so they are not conducive to determining the TD mobility relation. Since homogeneous nucleation is not the focus of our study, we do not investigate cases with $v_{predict}$ >5600 m/s further.

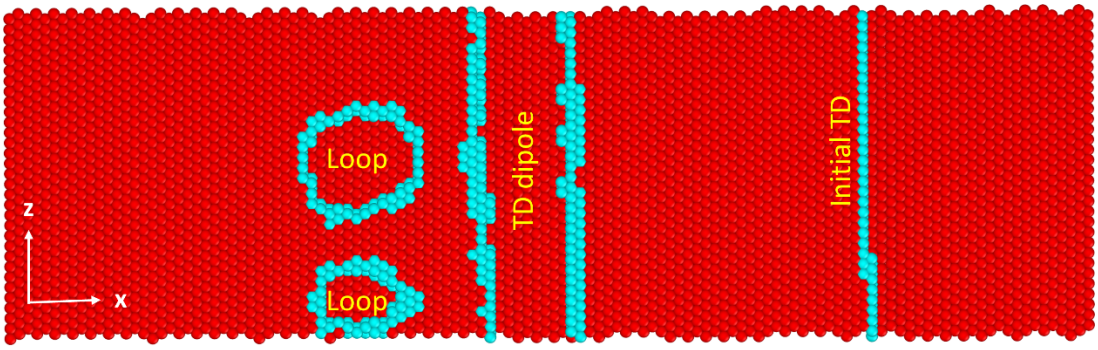

Figure 4: Dislocation loops and TD dipoles nucleated homogeneously within the CTB plane for TD moving at $v_{predict}$=5800m/s.

To obtain the mobility relation for the TD, we plotted the dislocation velocity against resolved shear stress for data sets from multiple simulations with predicted velocities ranging from 100 m/s to 5600 m/s. The outcome is shown in Fig. 5.a). The TD mobility relation is composed of two distinct velocity branches separated by a band of forbidden velocities. The low velocity branch asymptotically approaches a limit between the Rayleigh velocity and the first transverse sound speed. The high velocity branch has velocities ranging from 3500 m/s up to supersonic velocity of ~5700m/s, *i.e.*, greater than the longitudinal sound speed. Dislocation velocity is not a linear function of stress in either branch. The forbidden band corresponds to the range of predicted velocities where no steady-state motion occurs. Instead, cyclic motion is observed for these velocities.

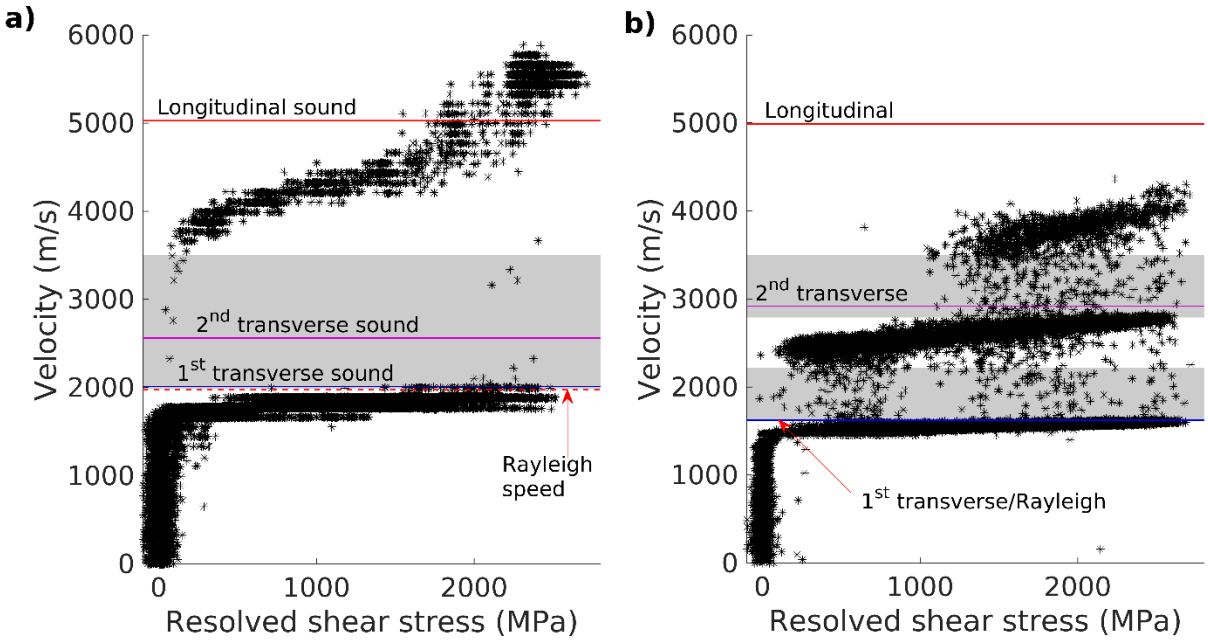

Figure 5: Mobility relations for a) a straight edge TD and b) an edge dislocation in pure FCC Cu (based on data from Ref. [33]). Regions shaded gray represent forbidden velocity bands.

For comparison, Fig. 5.b) shows the mobility relation for an edge dislocation in FCC Cu, based on data reported in Ref. [33]. Both the edge and TD mobility consist of distinct branches, meaning that dislocation velocity is not single-valued in stress for either of them. The subsonic part of both mobility relations in Fig. 5 is similar, with stress diverging at velocities near the Rayleigh velocities or first transverse sound speed. Both relations possess a high velocity branch, starting at around 3500-3600 m/s. However, for the TD, this branch extends over a wide range of stresses and up to supersonic speeds. Meanwhile, for the edge dislocation in FCC Cu, the high velocity branch extends over a narrower range of stresses and terminates well below the longitudinal sound speed. Finally, the mobility relation for an edge dislocation in FCC Cu possesses an intermediate velocity branch while the TD mobility relation does not.

We also assessed the effect of choosing different seed values when assigning initial velocities in our simulations. Three seeds were randomly selected in the range between 1 and 1,000,000,000. We used each seed to generate an ensemble of velocities at 10K. These velocities were used in simulations for TD motion with predicted velocity = 1430m/s. The simulation time was set to 2000ps. We computed the means and standard deviation of velocities and stresses for these three simulations. The outcomes are shown in Table 1 below. All the mean values were identical to within the standard error. We therefore conclude that our findings are robust with respect to different seed selections.

Table 1: Average instantaneous dislocation velocities and stresses for TD motion with predicted velocity = 1430 m/s given initial velocities assigned using different seed values.

Seed value	Velocity mean (m/s)	Stress mean (MPa)	Velocity standard deviation (m/s)	Stress standard deviation (MPa)
156954799	1430.12±3.28	9.13±1.24	103.79	39.48
780459496	1430.32±3.26	9.08±1.25	103.30	39.65
635657737	1430.71±3.25	9.05±1.26	103.10	39.78

4. Kink-mediated TD motion

Figure 6 compares the displacement as a function of time for TDs with and without a pre-existing kink at a predicted velocity of 1430 m/s. The TD without a kink exhibits cyclic stick-slip behavior: it alternates between ~0.1ps-long periods of motionlessness and ~0.05 ps bursts of high velocity, whereupon the TD translates by one Burgers vector magnitude, i.e., ~2 Å. By contrast, a TD with a pre-existing kink appears to translate continuously without any stick-slip behavior.

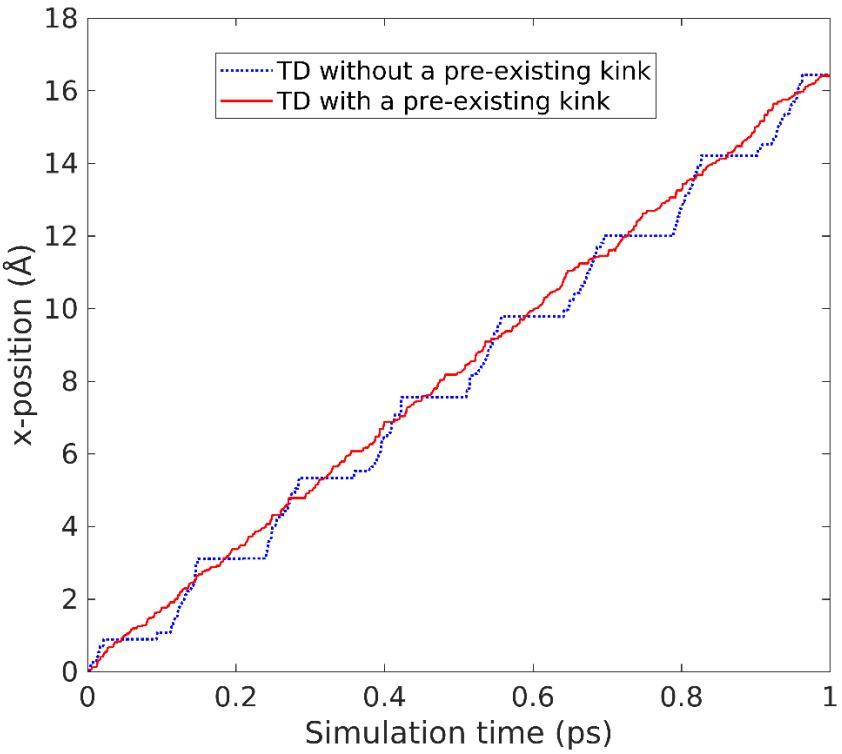

Figure 6: Position as a function of time for a TD with (blue dots) and without (solid red line) a pre-existing kink. Both dislocations move at an average predicted velocity of 1430 m/s.

The origin of this stick-slip behavior is apparent in Fig. 7, which shows snapshots of TD cores throughout one stick-slip cycle. Figure 7.a) presents a TD without a pre-existing kink at the beginning of the stick stage, defined as t=0 fs. The beginning of the slip stage, t=113 fs, is shown in Fig. 7.b). The TD core does not advance uniformly along its entire length. Rather, a kink pair forms and translates a small segment of the dislocation by one Burgers vector while the remainder of the

TD line remains static. Subsequently, the two kinks move in opposite directions, advancing the core position as shown in Fig. 7.c), while additional kink pairs are nucleated at other locations. Eventually, each kink meets and annihilates with an opposite sign kink, recovering a straight edge TD, as shown in Fig. 7.d), ending the stick-slip cycle. All other stick-slip cycles proceed through a similar sequence of events.

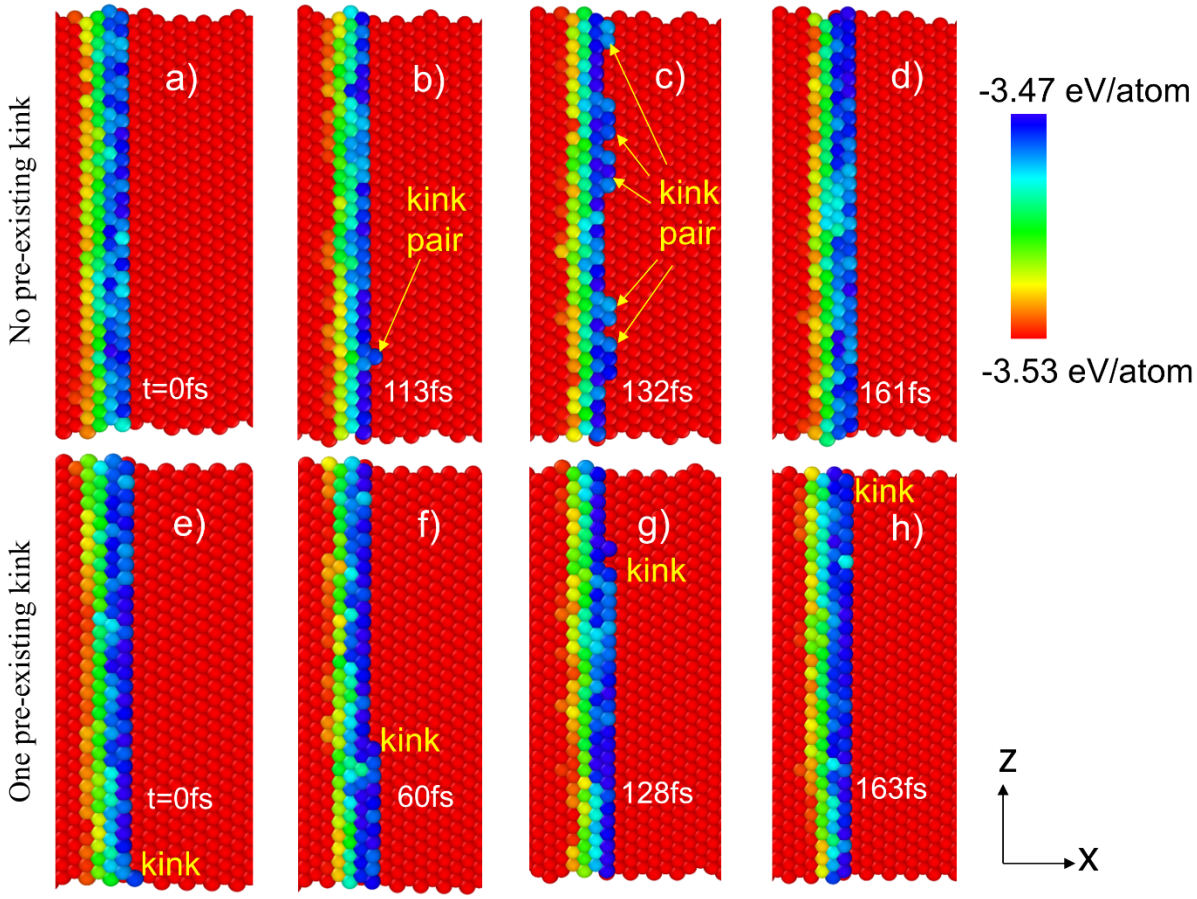

Figure 7: Core motion at predicted velocity of 1430 m/s for a TD a)-d) without and e)-h) with a pre-existing kink. Atoms are colored by potential energy.

By contrast, there is no double kink nucleation in the case of a TD with a pre-existing kink. As shown in Figs. 7.e)-h), the pre-existing kink simply translates at a uniform velocity. Thus, TD motion in Cu is kink mediated. An initially kink-free TD exhibits stick-slip behavior due to successive nucleation and annihilation of kink pairs.

However, kinks do not appear to have a major influence on the mobility relation of high-speed TDs. By way of illustration, Fig. 8 compares instantaneous TD velocities as a function of time for models with and without pre-existing kink for predicted velocity of 2503 m/s. Both models have the same cyclic behavior, two identical velocity branches, and similar variation in shear stress. The main difference between them is the duration of a single cycle: to complete the first cycle, a TD with no pre-existing kink needs 2337 ± 1 ps while a TD with a pre-existing kink requires only 2226 ±1 ps. Thus, it appears that kinks may make it easier for dislocations to transition between distinct branches of the mobility relation.

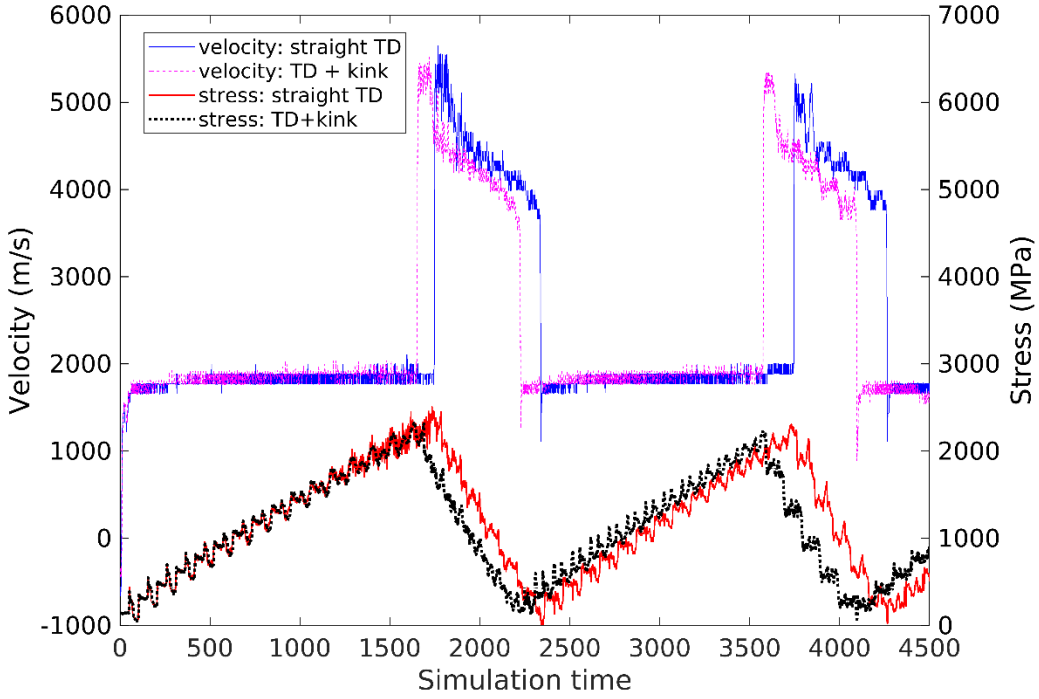

Figure 8: Instantaneous velocities and stresses of TDs with and without pre-existing kinks for predicted velocity of 2503 m/s.

5. Discussion

We have determined the mobility relation for a pure edge twinning dislocation (TD) in Cu. Our findings have direct bearing on the mobility of coherent twin boundaries (CTBs) as well as on the mobility of kinks on edge TDs. In our simulations, when a TD traverses a distance L_x on the glide plane, the CTB moves by one interatomic plane spacing, $a/\sqrt{3}$. Thus, the average velocities of the TD, v_{TD}, nd the CTB, v_{CTB}, are related by $\frac{a}{v_{CTB}\sqrt{3}} = \frac{L_x}{v_{TD}}$. Recognizing that the TD density per unit CTB area in our simulation is $\rho = 1/L_x$, we may write $v_{CTB} = v_{TD}\frac{a\rho}{\sqrt{3}}$. If $a\rho \ll 1$, it seems likely that propagation of twins at even modest fractions of the lower transverse sound speed involves sonic, transonic, or supersonic TD motion. Given that the maximum velocity a TD may sustain before onset of homogeneous dislocation nucleation is approximately three times the lower transverse sound speed, a twin boundary moving a sonic-level velocities implies both an extremely high TD velocity and an elevated TD density ($a\rho$ approaching unity).

Our modeling demonstrates that TDs of edge character propagate by kink motion. In our simulations, a TD advances by $a/\sqrt{6}$ (one Burgers vector magnitude) whenever a kink moves a distance L_z along TD line. Thus, the kink velocity v_{kink} obeys $\frac{a}{v_{TD}\sqrt{6}} = \frac{L_z}{v_{kink}}$. Writing $l = 1/L_z$ for the density of kinks per unit dislocation line, we conclude $v_{kink} = v_{TD}\frac{\sqrt{6}}{al}$. If $al \ll 1$, then kinks propagate significantly faster than TDs. Moreover, $v_{kink} = v_{CTB}\frac{3\sqrt{2}}{a^2\rho l}$, suggesting that TD kinks

propagate at sonic-level velocities even when CTB velocities are well below the transverse sound speed.

The mobility relation of a TD possesses two distinct branches separated by a velocity gap. As we explained in a previous publication [33], such structure in the mobility relation may be understood in terms of the velocity dependence of the drag force acting on a moving dislocation. Whenever the derivative of the drag force with respect to velocity is positive, uniform motion is stable. This condition holds within the two branches of the TD mobility shown in Fig. 5.a). Conversely, whenever the derivative is negative, uniform motion is not stable. Such is the case within the gap between the two branches in Fig. 5.a). The dislocation undergoes cyclic motion in that range of velocities. The foregoing implies that the slope of the drag force changes sign from positive to negative as TD velocity increases across the lower transverse sound speed. We therefore conclude that the drag force reaches a local maximum around the lower transverse sound speed. Similar to pure edge and screw dislocations in Cu [33], we attribute this behavior to a mechanical resonance of the moving dislocations with sound waves (at the lower transverse speed) as well as with Rayleigh surface waves (whose velocity is near the lower transverse sound speed in our model). We expect that such resonance leads to increased energy dissipation, e.g., through enhanced phonon scattering [48]. Our simulations do not permit us to conclude whether there is another peak in the drag force at supersonic velocities or if the drag force continues to increase monotonically with velocity beyond the longitudinal sound speed.

By contrast to TD, the mobility relation of a full edge dislocation in FCC Cu has three distinct branches. The middle velocity branch of a full edge dislocation, which lies just below the second transverse sound speed, is missing in the TD case. Previously, we explain that the middle branch of the edge dislocation mobility relation originates from a resonance between the dislocation and shear-horizontal (SH) waves [33]. SH waves [51, 52] involve atom displacements parallel to the free surfaces and perpendicular to the propagation direction, i.e., parallel to the dislocation line. We believe this middle branch is absent from the TD mobility relation because the elastic field of a pure edge TD has no component parallel to its line direction and therefore cannot interact with SH waves. By contrast, a full edge dislocation dissociates into Shockley partials, each of which has a screw component and is therefore capable of exciting a SH displacement field. Therefore, the absence of middle branch in the TD mobility relation is consistent with our interpretation of the role of SH waves in dislocation mobility.

In our simulations, cyclic motion arises from the constant strain rate loading condition. If an average velocity within the forbidden band is applied, this velocity cannot be accommodated by uniform dislocation motion. Instead, the dislocation achieves the average velocity by jumping between two steady state velocities: one in low velocity branch with $v < v_{predicted}$ and another in high velocity branch with $v > v_{predicted}$. While the dislocation is in the low velocity branch, the plastic strain rate (due to dislocation motion) is lower than the total applied strain rate. Thus, there is a residual elastic strain rate leading to a gradual increase in stress. The time spent by the dislocation in the lower velocity branch is determined by the time required for the stress to reach the threshold ~2.5 GPa at which the lower branch terminates. The dislocation then jumps to the higher velocity branch. Here, the plastic strain rate is greater than the total applied strain rate. Thus, the residual elastic strain rate leads to a gradual decrease in stress. The time spent by the dislocation in the higher velocity is determined by the time required to reach the lower stress limit of the higher branch, i.e., ~0.2 GPa. At this point, the TD jumps to the lower velocity branch. Cyclic behavior is not expected under constant stress [15, 16].

In contrast to full edge dislocations, the mobility relation of a TD extends into the supersonic regime. This observation is consistent with the previous work of Daphalapurkar *et al.*, who investigated TDs in Ni (FCC) [23]. Supersonic motion has also been reported for edge dislocations in tungsten (BCC) [18, 21] and silicon (diamond cubic) [53]. However, all these previous reports suggest that there is a gap of forbidden velocities separating the transonic and supersonic regimes [18, 21, 23]. Thus, to reach supersonic speed, dislocations must either accelerate rapidly across this gap or nucleate already possessing supersonic velocity. Instead, we find that the upper mobility branch of a TD in Cu extends continuously from the transonic to the supersonic regime, meaning that a TD may cross the longitudinal sound speed while undergoing uniform motion.

Compared to pure edge and pure screw dislocations in Cu, TDs are the most mobile: they achieve the highest speeds at lowest resolved shear stress. The highest shear stress and velocity of a TD are ~2.5GPa and 5800m/s, respectively. By contrast, those values are ~2.6GPa and 3600m/s for a pure edge and 3.2GPa and 2500m/s for a pure screw dislocation in Cu [33].

We find that motion of pure edge TDs in Cu is mediated by kinks. A stick-slip cycle of a TD with no pre-existing kinks requires ~160 fs to complete. It resembles the motion of dislocations with compact cores moving in the 2-D models of Koizumi *et al.* [54]. In their simulations, a screw dislocation undergoes cyclic stick-slip motion, with travel distance of one Burgers vector during each slip increment, as in our simulations. However, due to the 2-D geometry used by Koizumi *et al.*, their model does not involve kink motion or double kink nucleation. Stick-slip motion has been reported for twin boundary migration, but its origins also are not from double-kink nucleation. For example, Verma *et al.* [55] found that stick-slip motion of an incoherent Σ3 grain boundary in a Cu alloy is due to thermally assisted interactions with solutes. Hu *et al.* [56] investigated the migration of a CTB in copper and found stick-slip cycles lasting in the order of 20-50 ps due to nucleation of twinning dislocations from free surfaces.

While the kink-mediated character of TD motion does not have a major effect on TD mobility at the high velocities investigated here, we anticipate that it may be relevant for the motion of TDs at resolved stresses below the Peierls threshold. In particular, it may impart to TDs a temperature dependence similar to that of screw dislocations in BCC metals, whose motion is also kink-mediated [57-59].

We investigated the mobility of a single edge TD. However, translation of some twin boundaries involves the concurrent motion of several TDs. For example, Wang et *al*. [60] showed that Σ3 symmetric incoherent twin boundaries (SITBs) in Cu consist of triplets of Shockley partial twinning dislocations, including one pure edge and two of mixed edge/screw character. The mobility of such groupings may differ from that of a single TD, both because of the variety of dislocation characters involved as well as due to interactions among the moving TDs. Future investigations could consider such effects, both for SITBs as well as other twin boundary types.

Experimental investigations of sonic-level twin motion remain challenging and nearly always involve numerous assumptions. For example, Gray did not measure instantaneous velocities of twin boundaries [1], but rather calculated average velocities based on twin displacements. This calculation assumes uniform, unidirectional motion of the twin plane as well as no nucleation or coalescence of twin segments. Due to low time resolution (0.96 μs), the experiment of Faran and Shilo results in a large uncertainty of the twin velocity [2]. Time resolved measurements using x-ray free-electron lasers (XFEL) may provide a means of observing instantaneous velocities of sonic, transonic, and supersonic twins and TDs. Katagiri *et al.* report transonic dislocation motion in diamond using this technique [14]. However, the range of materials that may currently be investigated by the XFEL is limited by the energy and flux of available light sources [61].

6. Conclusion

We have investigated the mobility of a high-speed edge twinning dislocation (TD) in Cu using molecular dynamics. We find that the mobility relation consists of two discrete branches. One is subsonic: it begins at zero velocity and terminates below the first transverse sound speed of ~2000 m/s. The other spans from a transonic velocity 3500 m/s to a supersonic velocity 5700 m/s.

For a velocity within either these two branches, the TD undergoes uniform motion, where velocity and stress oscillate about constant values. By contrast, if an average velocity is imposed that falls within the gap between the two branches, 2000 m/s$< v <$ 3500 m/s, the dislocation jumps cyclically between the lower and upper velocity branches while the stress alternates between continuously increasing (while the TD velocity is in the lower branch) to continuously decreasing (TD velocity in the upper branch).

Our simulations show that the motion of an edge TD in Cu is kink mediated. Kink-pair nucleation is required to move a TD that does not contain any pre-existing kinks. There is no apparent difference in the mobility relation for TDs with and without kinks at the high velocities investigated here.

Acknowledgements

This work was supported by the Department of Energy, National Nuclear Security Administration, under award no. DE-NA0003857. Computing resources were provided by the High Performance Research Computing (HPRC) center at Texas A&M University. This work was performed, in part, at the Center for Integrated Nanotechnologies, an Office of Science User Facility operated for the U.S. Department of Energy. RD is supported by the United States (U.S.) Department of Energy (DOE) Office of Basic Energy Sciences (BES), Division of Materials Science and Engineering.

This article has been authored by an employee of National Technology & Engineering Solutions of Sandia, LLC under Contract No. DE-NA0003525 with the U.S. DOE. The employee owns all right, title and interest in and to the article and is solely responsible for its contents. The United States Government retains and the publisher, by accepting the article for publication, acknowledges that the United States Government retains a non-exclusive, paid-up, irrevocable, world-wide license to publish or reproduce the published form of this article or allow others to do so, for United States Government purposes. The DOE will provide public access to these results of federally sponsored research in accordance with the DOE Public Access Plan: https://www.energy.gov/downloads/doe-public-access-plan.

References:

[1] G.T. Gray III, Deformation twinning in Al-4.8 wt% Mg, Acta Metallurgica 36(7) (1988).
[2] E. Faran, D. Shilo, Twin motion faster than the speed of sound, Physical Review Letters 104 (2010).
[3] J.W. Christian, S. Mahajan, Deformation twinning, Progress in Materials Science 39 (1995) 1-157.
[4] J.P. Hirth, J. Lothe, Theory of dislocations, Krieger Publishing Company 1982.
[5] W.G. Johnston, J.J. Gilman, Dislocation velocities, dislocation densities, and plastic flow in lithium fluoride crystals, Journal of Applied Physics 30(2) (1959) 129-144.
[6] K.M. Jassby, T. Vreeland, An experimental study of the mobility of edge dislocations in pure copper single crystals, Philosophical Magazine 21(174) (1970) 1147-1168.
[7] K.M. Jassby, T. Vreeland, Dislocation mobility in copper and zinc at 44K, Scripta Metallurgica 5 (1971).
[8] K. Marukawa, Dislocation motion in copper single crystals, Journal of Physical Society of Japan 22(2) (1967) 499-510.
[9] M. Wada, M. Meshii, K. Marukawa, Dislocation velocity in copper electron irradiated at 100 K, Physica Status Solidi (a) 57(1) (1980) 345-354.
[10] M. Kleintges, R. Labusch, H.G. Brion, P. Haasen, Measurement of dislocation velocities in Cu-Al single crystals -I, Acta Metallurgica 25 (1977).
[11] A.P.L. Turner, T. Vreeland, The effect of small concentrations of carbon impurity on dislocation mobility in iron monocrystals Scripta Metallurgica 4 (1970).
[12] J. Cotner, J. Weertman, High dislocation velocities and the structures of slip bands in shock loaded high purity lithium fluoride, Discussions of the Faraday Society 38 (1964) 225-232.
[13] V. Nosenko, G.E. Morfill, P. Rosakis, Direct experimental measurement of the speed-stress relation for dislocations in a plasma crystal, Phys Rev Lett 106(15) (2011) 155002.
[14] K. Katagiri, T. Pikuz, L. Fang, B. Albertazzi, S. Egashira, Y. Inubushi, G.K.R. Kodama, M. Koenig, B. Kozioziemski, G. Masaoka, K. Miyanishi, H.N.M. Ota, G. Rigon, Y.S.T. Sano, F. Schoofs, Z.J. Smith, K. Sueda, T.T.T. Vinci, Y. Wang, M.Y.T. Yabuuchi, L.E.D. Marais, N. Ozaki, Transonic dislocation propagation in diamond, Science 382 (2023) 69-72.
[15] J. Marian, A. Caro, Moving dislocations in disordered alloys: Connecting continuum and discrete models with atomistic simulations, Physical Review B 74(2) (2006).
[16] D.L. Olmsted, L.G. Hector Jr, W.A. Curtin, R.J. Clifton, Atomistic simulations of dislocation mobility in Al, Ni and Al/Mg alloys, Modelling and Simulation in Materials Science and Engineering 13(3) (2005) 371-388.
[17] Z. Jin, H. Gao, P. Gumbsch, Energy radiation and limiting speeds of fast moving edge dislocations in tungsten, Physical Review B 77(9) (2008).
[18] Q. Li, S.-Q. Shi, Dislocation jumping over the sound barrier in tungsten, Applied Physics Letters 80(17) (2002) 3069-3071.
[19] D. Mordehai, Y. Ashkenazy, I. Kelson, G. Makov, Dynamic properties of screw dislocations in Cu: A molecular dynamics study, Physical Review B 67(2) (2003).
[20] E. Oren, E. Yahel, G. Makov, Dislocation kinematics: a molecular dynamics study in Cu, Modelling and Simulation in Materials Science and Engineering 25(2) (2017).
[21] P. Gumbsch, H. Gao, Dislocations faster than speed of sounds, Science 283 (1999) 965-968.
[22] S. Peng, Y. Wei, Z. Jin, W. Yang, Supersonic Screw Dislocations Gliding at the Shear Wave Speed, Phys Rev Lett 122(4) (2019) 045501.

[23] N.P. Daphalapurkar, J.W. Wilkerson, T.W. Wright, K.T. Ramesh, Kinetics of a fast moving twin boundary in nickel, Acta Materialia 68 (2014) 82-92.
[24] Y. Wei, S. Peng, The stress-velocity relationship of twinning partial dislocations and the phonon-based physical interpretation, Science China Physics, Mechanics & Astronomy 60(11) (2017).
[25] J. Wang, N. Li, O. Anderoglu, X. Zhang, A. Misra, J.Y. Huang, J.P. Hirth, Detwinning mechanisms for growth twins in face-centered cubic metals, Acta Materialia 58(6) (2010) 2262-2270.
[26] A. Verma, O.K. Johnson, G.B. Thompson, I. Chesser, S. Ogata, E.R. Homer, Insights into factors that affect non-Arrhenius migration of a simulated incoherent Σ3 grain boundary, Acta Materialia 258 (2023).
[27] R.B. Sills, S. Aubry, Line dislocation dynamics simulations with complex physics., in: W. Andreoni, S. Yip (Eds.), Handbook of Materials Modeling, Springer2020, pp. 1559-1581.
[28] R. LeSar, L. Capolungo, Advances in discrete dislocation dynamics simulations, in: W. Andreoni, S. Yip (Eds.), Handbook of Materials Modeling: Methods: Theory and Modeling, Springer2020, pp. 1079-1110.
[29] Y. Cui, T. Wang, S. Luo, Z. Li, Z. Li, A discrete–continuous model of three-dimensional dislocation elastodynamics, International Journal of Plasticity 152 (2022).
[30] J. Cho, J.F. Molinari, G. Anciaux, Mobility law of dislocations with several character angles and temperatures in FCC aluminum, International Journal of Plasticity 90 (2017) 66-75.
[31] B. Gurrutxaga-Lerma, The role of the mobility law of dislocations in the plastic response of shock loaded pure metals, Modelling and Simulation in Materials Science and Engineering 24 (2016).
[32] Y. Mishin, M.J. Mehl, D.A. Papaconstantopoulos, A.F. Voter, J.D. Kress, Structural stability and lattice defects in copper: Ab initio, tight-binding, and embedded-atom calculations, Physical Review B 63(22) (2001).
[33] T. Duong, M.J. Demkowicz, Resonance with surface waves induces forbidden velocity bands in dislocation glide, Journal of the Mechanics and Physics of Solids 180 (2023).
[34] N. Li, J. Wang, A. Misra, X. Zhang, J.Y. Huang, J.P. Hirth, Twinning dislocation multiplication at a coherent twin boundary, Acta Materialia 59(15) (2011) 5989-5996.
[35] W.Z. Han, Z.F. Zhang, S.D. Wu, S.X. Li, Combined effects of crystallographic orientation, stacking fault energy and grain size on deformation twinning in fcc crystals, Philosophical Magazine 88(24) (2008) 3011-3029.
[36] X.X. Wu, X.Y. San, Y.L. Gong, L.P. Chen, C.J. Li, X.K. Zhu, Studies on strength and ductility of Cu–Zn alloys by stress relaxation, Materials & Design 47 (2013) 295-299.
[37] A.P. Thompson, H.M. Aktulga, R. Berger, D.S. Bolintineanu, W.M. Brown, P.S. Crozier, P.J. in 't Veld, A. Kohlmeyer, S.G. Moore, T.D. Nguyen, R. Shan, M.J. Stevens, J. Tranchida, C. Trott, S.J. Plimpton, LAMMPS - a flexible simulation tool for particle-based materials modeling at the atomic, meso, and continuum scales, Computer Physics Communications 271 (2022).
[38] M.S. Daw, M.I. Baskes, Embedded-atom method: Derivation and application to impurities, surfaces, and other defects in metals, Physical Review B 29(12) (1984) 6443-6453.
[39] H. Tsuzuki, P.S. Branicio, J.P. Rino, Molecular dynamics simulation of fast dislocations in copper, Acta Materialia 57(6) (2009) 1843-1855.
[40] A. Stukowski, Visualization and analysis of atomistic simulation data with OVITO–the Open Visualization Tool, Modelling and Simulation in Materials Science and Engineering 18(1) (2010).

[41] H. Tsuzuki, P.S. Branicio, J.P. Rino, Structural characterization of deformed crystals by analysis of common atomic neighborhood, Computer Physics Communications 177(6) (2007) 518-523.
[42] M.C. Inman, A.R. Khan, The interfacial energy of coherent twin boundarier in copper, Philosophical Magazine 6(37) (1961) 637-638.
[43] M.A. Tschopp, D.L. McDowell, Structures and energies of Σ 3 asymmetric tilt grain boundaries in copper and aluminium, Philosophical Magazine 87(22) (2007) 3147-3173.
[44] A.S. Argon, Strengthening mechanisms in crystal plasticity, Oxford University Press 2008.
[45] D.J. Bacon, D.M. Barnett, R.O. Scattergood, Anisotropy lattice defect theory, Progress in Materials Science 23 (1979).
[46] D.N. Blaschke, How to determine limiting velocities of dislocations in anisotropic crystals, Journal of Physics: Condensed Matter 33(50) (2021).
[47] D.N. Blaschke, T. Duong, M.J. Demkowicz, Comparing theoretical predictions of radiation-free velocities of edge dislocations to molecular dynamics simulations, Physical Review B 108(22) (2023).
[48] V.I. Alshits, The phonon-dislocation interaction and its role in dislocation dragging and thermal resistivity, in: V.L. Indenbom, J. Lothe (Eds.), Elastic strain fields and dislocation mobility1992, p. 625.
[49] L.J. Teutonico, Uniformly Moving Dislocations of Arbitrary Orientation in Anisotropic Media, Physical Review 127(2) (1962) 413-418.
[50] J. Weertman, Fast Moving Edge Dislocations on the 111) Plane in Anisotropic Face-Centered-Crystals, Journal of Applied Physics 63 (1962).
[51] J.D. Achenbach, Wave propagation in elastic solids, North-Holland Publishing Company 1973.
[52] J.L. Rose, Ultrasonic guided waves in solid media, Cambridge University Press 2014.
[53] E.N. Hahn, S. Zhao, E.M. Bringa, M.A. Meyers, Supersonic dislocation bursts in silicon, Scientific Reports 6 (2016) 26977.
[54] H. Koizumi, H.O.K. Kirchner, T. Suzuki, Lattice wave emission from a moving dislocation, Physical Review B 65(21) (2002).
[55] A. Verma, O.K. Johnson, G.B. Thompson, S. Ogata, E.R. Homer, Solute influence in transitions from non-Arrhenius to stick-slip Arrhenius grain boundary migration, Acta Materialia 265 (2024).
[56] Q. Hu, L. Li, N.M. Ghoniem, Stick-slip dynamics of coherent twin boundary in copper, Acta Materialia 57 (2009).
[57] V. Vitek, Theory of the core structures of dislocations in body-centred-cubic metals, Crystal Lattice Defects 5(1) (1974) 1-34.
[58] C. Deo, D. Srolovitz, W. Cai, V. Bulatov, Stochastic simulation of dislocation glide in tantalum and Ta-based alloys, Journal of the Mechanics and Physics of Solids 53(6) (2005) 1223-1247.
[59] L. Dezerald, L. Proville, L. Ventelon, F. Willaime, D. Rodney, First-principles prediction of kink-pair activation enthalpy on screw dislocations in bcc transition metals: V, Nb, Ta, Mo, W, and Fe, Physical Review B 91(9) (2015).
[60] J. Wang, O. Anderoglu, J.P. Hirth, A. Misra, X. Zhang, Dislocation structures of Σ3 {112} twin boundaries in face centered cubic metals, Applied Physics Letters 95(2) (2009).
[61] M.D. Knudson, C.T. Seagle, Damaging diamond with shock waves, Science 382(6666) (2023) 37.

Appendix A: Recovery of perfect stacking during TD construction

Figure A1.a) shows a single $(11\bar{2})$ plane of atoms. The length of the periodic translations within the plane in $[111]$ and $[1\bar{1}0]$ are $a\sqrt{3}$ and $a\sqrt{2}/2$, respectively, where a is the cubic lattice parameter. In FCC solids, $(11\bar{2})$ planes are stacked in a six-fold sequence, as shown in Fig. A1.b). Each successive plane is translated relative to the previous one by $\vec{d}_2 = a\frac{\sqrt{3}}{3}\hat{\jmath}$ in the $[111]$ direction and by $\vec{d}_3 = a\frac{\sqrt{2}}{4}\hat{k}$ in $[1\bar{1}0]$. The distance between successive planes in the $[11\bar{2}]$ direction is $\vec{d}_1 = a\frac{\sqrt{6}}{12}\hat{\imath}$. Here, $\hat{\imath}$, $\hat{\jmath}$, and $\hat{k}$ are unit vectors in a Cartesian coordinate system aligned with the aforementioned crystallographic directions. Note that the periodic repeat distances within a single plane (Fig. A1.a)) are $3\vec{d}_2$ in the $[111]$ direction and $2\vec{d}_3$ in the $[1\bar{1}0]$ direction.

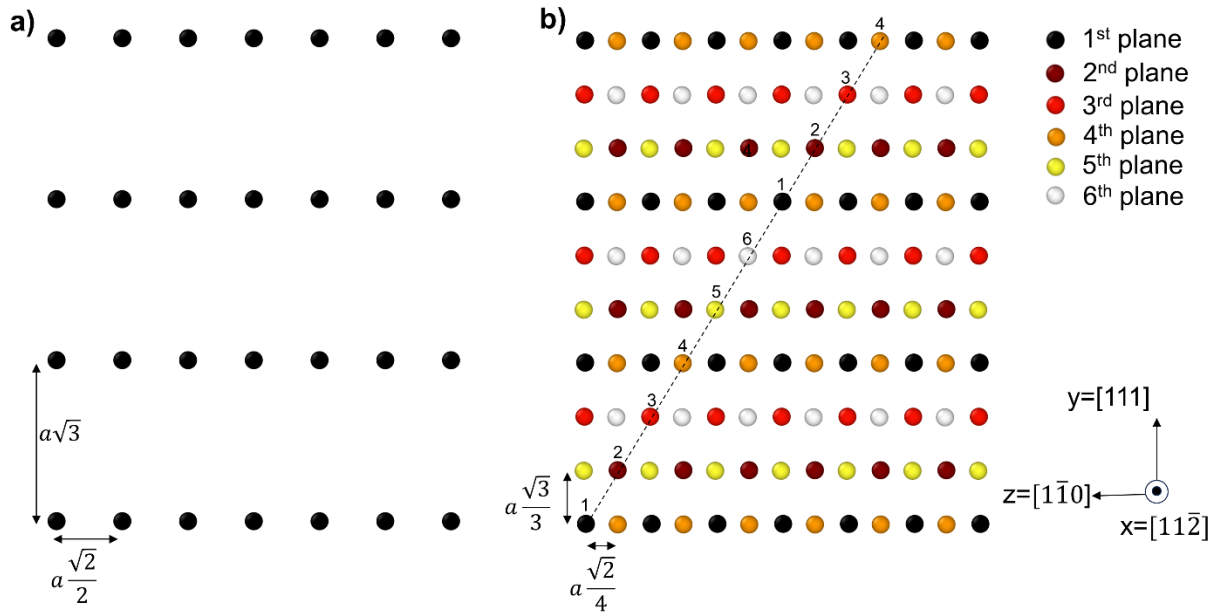

Fig. A1: Plan view of a) a single $(11\bar{2})$ plane and b) a complete, six-fold stacking of $(11\bar{2})$ planes. Atoms with the same color are from a single $(11\bar{2})$ plane, e.g., black atoms from the top-most $(11\bar{2})$ plane and white atoms from the bottom-most plane.

Consider the operation of removing a certain number, N, of $(11\bar{2})$ planes from a perfect FCC crystal followed by closing the resulting gap, as illustrated in Fig. A2.a). If N=6 (or any multiple thereof), this operation recovers perfect FCC stacking. For other values of N, simply closing the gap results in a stacking fault, as illustrated in Fig. A2.b) for N= 2. Perfect stacking may nevertheless be recovered if one side of the crystal is translated parallel to the $[111]$ and $[1\bar{1}0]$ directions by an appropriate multiple of $\vec{d}_2$ and $\vec{d}_3$, respectively. For example, Fig. A2.c) shows a perfect FCC crystal recovered after removing two $(11\bar{2})$ planes (N=2) and applying a displacement of $\vec{d}_2$ to the half crystal on the right of the gap. In a model under periodic boundary conditions, closing this gap and applying a relative translation between periodic images to restore perfect stacking

may be accomplished by adjusting the length and direction of the simulation cell continuation vector $\vec{A}$, as illustrated in Fig. A2.d), while the positions of atoms in the model remain fixed.

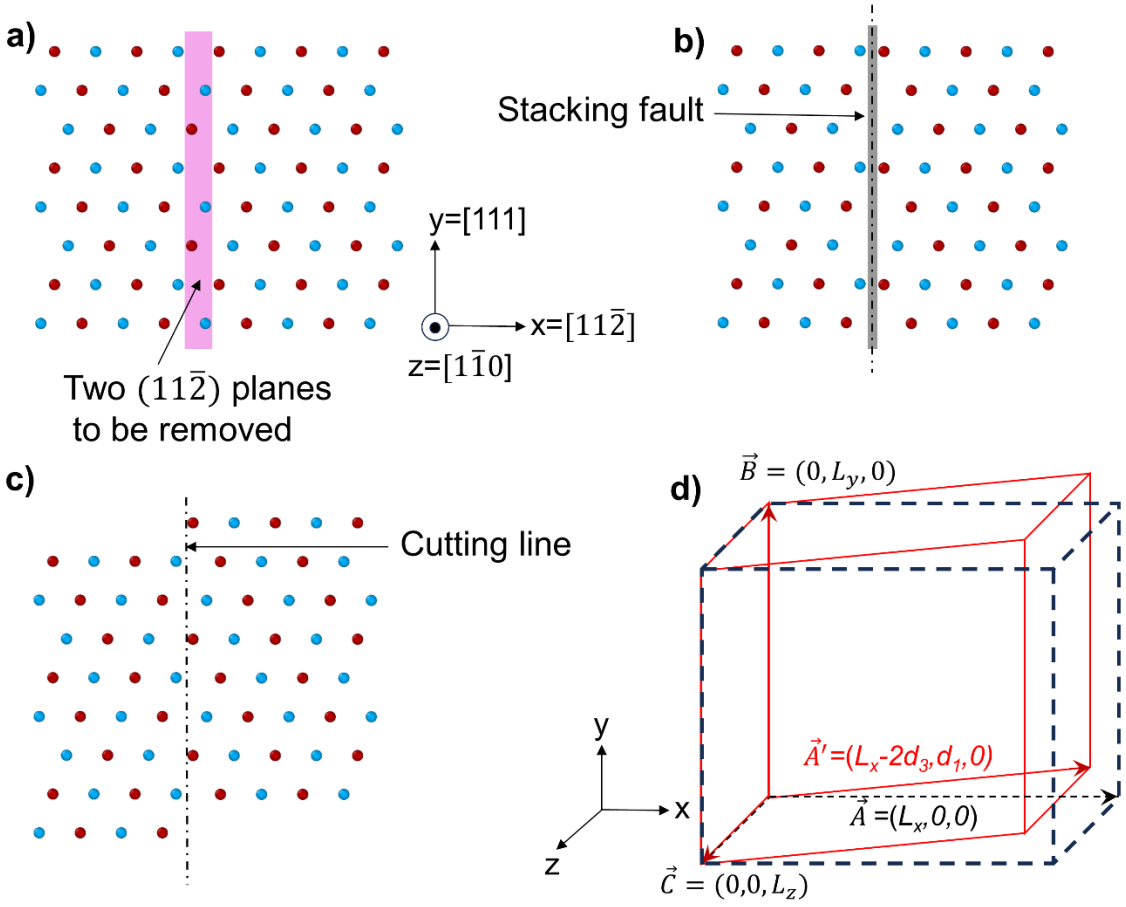

Fig. A2: Stacking sequence recovery after removing two $(11\bar{2})$ planes. a) Edge-on view of two $(11\bar{2})$ planes to be removed (highlighted in purple). b) A stacking fault along the cutting line after closing the gap created by the removal of two planes. c) Correct stacking recovered by imposing a shift of $\vec{d}_2$ in the [111] direction on the right block. In a), b), and c), atoms with the same color are from the same $(1\bar{1}0)$ plane. d) Under periodic boundary conditions, closing the gap created by removal of two $(11\bar{2})$ planes and imposing a relative shift to restore perfect stacking may be accomplished by altering the simulation cell shape while keeping atomic coordinates fixed. If the initial cell is orthorhombic (black dashed lines), the final one is triclinic (red solid lines).

To introduce an edge twinning dislocation into our CTB model, we must remove two more $(11\bar{2})$ planes from the crystal above the CTB than from the crystal below the CTB (so that the net closure failure is that of a single Shockley partial dislocation). Moreover, we wish to restore perfect FCC stacking in both crystals under periodic boundary conditions with a single set of shift vectors parallel to the $(11\bar{2})$ plane. This objective can only be accomplished for certain specific numbers of $(11\bar{2})$ planes removed from the top crystal.

Table A1 lists the shift vectors required to restore the stacking sequence for any value of N of planes removed from the bottom crystal as well for N+2 planes removed from the top crystal. Not all values of N allow for the stacking sequence to be recovered both above and below the CTB.

For example, when N=0, no shift is needed in the bottom crystal while a shift of $-\vec{d}_2$ is needed in the top crystal. Table A1 shows that the stacking sequence can be recovered for N=2 (which is the choice we used to construct our model) or N=5.

Table A1: Shifts that must be applied to the crystal above and below the CTB to restore the FCC stacking sequence. Rows shaded blue correspond to combinations of $(11\bar{2})$ plane removals that permit the correct stacking sequence to be recovered simultaneously in both top and bottom crystals with the same shift vectors.

N for the crystal below the CTB	**Shift needed to restore stacking in the crystal below the CTB**	**N+2 for the crystal above the CTB**	**Shift needed to restore stacking in the crystal above the CTB**
0	0	2	$-\vec{d}_2$
1	$-\vec{d}_2 - \vec{d}_3$	3	$-\vec{d}_3$
2	$\vec{d}_2$	4	$\vec{d}_2$
3	$-\vec{d}_3$	5	$-\vec{d}_2 - \vec{d}_3$
4	$-\vec{d}_2$	6	0
5	$\vec{d}_2 - \vec{d}_3$	7	$\vec{d}_2 - \vec{d}_3$
6	0	8	$-\vec{d}_2$